

Article

# Adapting the MgO-CO<sub>2</sub> Working Pair for Thermochemical Energy Storage by Doping with Salts: Effect of the (LiK)NO<sub>3</sub> Content <sup>†</sup>

Seon Tae Kim <sup>1,\*</sup> , Haruka Miura <sup>1</sup>, Hiroki Takasu <sup>1</sup>, Yunitaka Kato <sup>1</sup>, Alexandr Shkatulov <sup>2</sup> and Yuri Aristov <sup>1,3</sup>

<sup>1</sup> Tokyo Institute of Technology, 2-12-1-N1-22, Ōokayama, Meguro-ku, Tokyo 152-8550, Japan; miura.h.al@m.titech.ac.jp (H.M.); takasu.h.aa@m.titech.ac.jp (H.T.); yunitaka@lane.iir.titech.ac.jp (Y.K.); aristov@catalysis.ru (Y.A.)

<sup>2</sup> Department of Applied Physics, Eindhoven University of Technology, De Rondon 70, 5612 AP Eindhoven, The Netherlands; a.shkatulov@tue.nl

<sup>3</sup> Boreskov Institute of Catalysis, Ac. Lavrentiev av. 5, Novosibirsk 630090, Russia

\* Correspondence: kim.s.ag@m.titech.ac.jp

<sup>†</sup> The original paper was presented in: Shkatulov, A.I., Kim, S.T., Kato, Y., Aristov, Yu.I. Adapting the MgO-CO<sub>2</sub> working pair for thermochemical energy storage by doping with salts. Riehl, R., Preißinger, M., Eames, I., Tierney, M., Eds. In Proceedings of the Heat Powered Cycles Conference 2018, Bayreuth, Germany, 16–19 September 2018; ISBN 978-0-9563329-6-7.

Received: 30 April 2019; Accepted: 11 June 2019; Published: 13 June 2019



**Abstract:** The MgO-CO<sub>2</sub> working pair has been regarded as prospective for thermochemical energy storage (TCES) due to its relatively high heat storage capacity, low cost, and wide availability. This study is aimed at the optimization of the molar salt content,  $\alpha$ , for the MgO modified with the eutectic mixture of LiNO<sub>3</sub> and KNO<sub>3</sub> (Li<sub>0.42</sub>K<sub>0.58</sub>NO<sub>3</sub>) which was earlier shown to provide high conversion,  $\Delta x$ , in heat-storage/release processes at 300–400 °C. The composites that have different salt content were prepared and carbonation kinetics was investigated under various conditions (carbonation temperature,  $T_{\text{carb}}$ , is 290–360 °C and CO<sub>2</sub> pressure,  $P(\text{CO}_2)$ , is 50–101 kPa). Significant accelerating effect was revealed at  $\alpha \geq 0.05$ , and the  $\Delta x$  value was maximized at  $\alpha = 0.10$ – $0.20$ . The largest conversion of 0.70 was detected at  $\alpha = 0.10$  and  $T_{\text{carb}} = 350$  °C that corresponds to the specific useful heat ( $Q_{\text{comp}}$ ) is 1.63 MJ/kg-composite. However, the salt content of 0.20 ensures the high conversion,  $\Delta x = 0.63$ – $0.67$  and  $Q_{\text{comp}} = 1.18$ – $1.25$  MJ/kg-composite in the whole temperature range between 290 and 350 °C. The (LiK)NO<sub>3</sub>/MgO composite with an optimal salt content of 0.20 exhibits reasonable durability through cyclic experiment at 330 °C, namely, the stabilized reacted conversion  $\Delta x = 0.34$  ( $Q_{\text{comp}} = 0.64$  MJ/kg-composite). The studied (Li<sub>0.42</sub>K<sub>0.58</sub>)NO<sub>3</sub> promoted MgO-CO<sub>2</sub> working pair has good potential as thermochemical storage material of middle temperature heat (300–400 °C).

**Keywords:** thermochemical energy storage; magnesium oxide; magnesium carbonate; salt modification; eutectic mixture

## 1. Introduction

Storage of thermal energy by means of chemical reactions with high heat effect, or thermochemical energy storage (TCES), is a promising approach to convert primary energy source due to high thermal energy storage capacity and long-term storage at ambient temperature without insulation [1–3]. To the date, chemical reactions that can be neatly applied to TCES at medium temperatures (200–500 °C) to store heat from industrial and renewable (e.g., solar energy) sources are not numerous. Aside from large-scale industrial processes such as ammonia production [4] there are only a few solid-gas reactions

that were extensively studied specifically for TCES at medium temperatures. They are dehydration of  $\text{Mg}(\text{OH})_2$  [5],  $\text{Ca}(\text{OH})_2$  [6], dehydrogenation of  $\text{MgH}_2$  and some other hydrides [7].

The carbonation of  $\text{MgO}$ , Equation (1), that has the high reaction enthalpy, 116.4 kJ/mol, and suitable equilibrium temperature,  $T_{eq} = 388 \text{ }^\circ\text{C}$  (at  $P(\text{CO}_2) = 101 \text{ kPa}$ ), was considered for TCES since the late 70s [8].

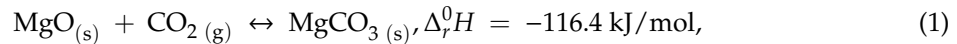
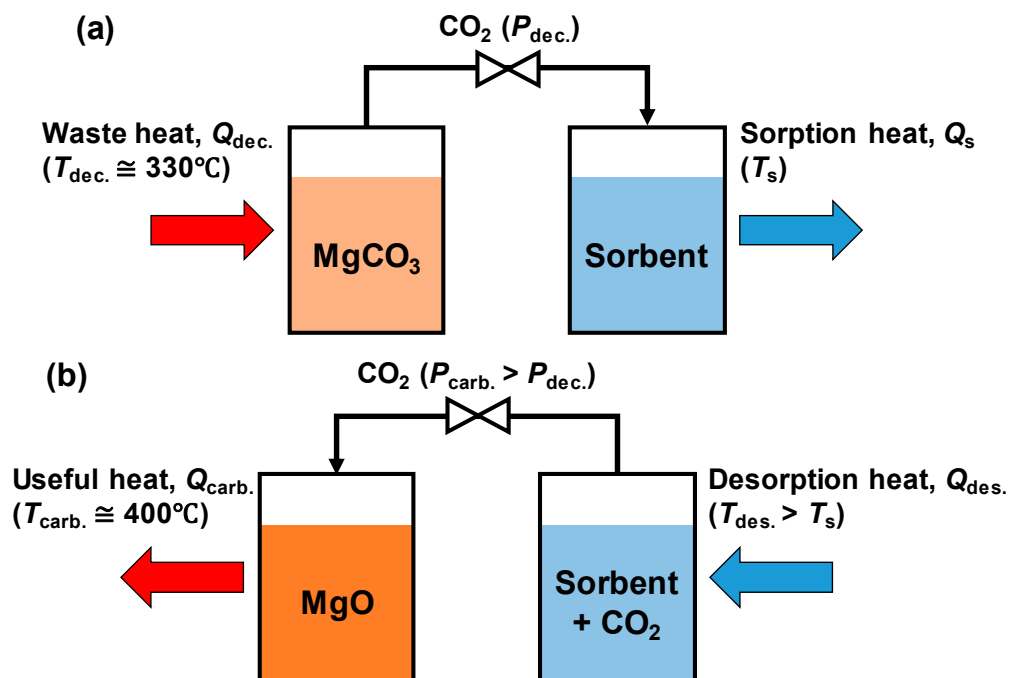


Figure 1 shows the principle of a  $\text{MgO}/\text{CO}_2/\text{sorbent}$  TCES system. For heat storage,  $\text{MgCO}_3$  is decomposed by supplied heat energy,  $Q_{dec.}$  at temperature,  $T_{dec.}$ , of 300–350 °C (the backward reaction in Equation (1)). The products ( $\text{MgO}$  and  $\text{CO}_2$ ) are separated and decomposed  $\text{CO}_2$  moves into the sorbent reactor with generating heat of sorption,  $Q_s$ ; the heat is stored in a chemical form for theoretically infinite time (Figure 1a). In the heat release process, the  $\text{CO}_2$  desorbed by desorption heat,  $Q_{des.}$  is supplied to  $\text{MgO}$  reactor then generates heat energy,  $Q_{carb.}$ , (the forward reaction in Equation (1)) at temperature,  $T_{carb.}$ , of ~400 °C (Figure 1b). Usually, carbonation pressure,  $P_{carb.}$ , and desorption temperature,  $T_{des.}$ , are higher than decarbonation pressure,  $P_{dec.}$ , and temperature of sorption heat,  $T_s$ , respectively.



**Figure 1.** Principle of  $\text{MgO}/\text{CO}_2/\text{sorbent}$  TCES system. (a) Heat storage process by  $\text{MgCO}_3$  decarbonation. (b) Heat output process by  $\text{MgO}$  carbonation.

Although there are many thermodynamic advantages to  $\text{MgO}$  carbonation, TCES systems using this reaction have rarely been reported in reviews dedicated to TCES [9–12]. The reason is a strong irreversibility of reaction as the interaction of  $\text{MgO}$  with  $\text{CO}_2$  is kinetically hindered [13,14] that makes a return of the stored heat practically impossible. Due to this, the first detailed study of the  $\text{MgO}-\text{CO}_2$  working pair has appeared only recently [15]. The authors made a brief screening of salt additives to pure  $\text{MgO}$  with the aim to find a salt which increases the oxide reactivity towards carbonation. They used a powerful salt modification approach earlier suggested and tested for TCES at middle temperatures in many papers such as  $\text{LiCl}$  for hydration of  $\text{MgO}$  [16], metal nitrates for doping of  $\text{MgO}$  [17,18], and  $\text{Li}$  for hydration of  $\text{CaO}$  [19,20]. This approach was also successfully applied to synthesize  $\text{MgO}$ -based sorbents for intermediate-temperature  $\text{CO}_2$  capture [21] and high-temperature heat storage systems [9].

In total, eight salts with MgO (salt content 10 mol%) were prepared and investigated in [15]. It was found that  $\text{CH}_3\text{COOLi}$  and  $\text{Li}_{0.42}\text{K}_{0.58}\text{NO}_3$  considerably promote the MgO carbonation. The eutectic mixture  $\text{Li}_{0.42}\text{K}_{0.58}\text{NO}_3$  of  $\text{LiNO}_3$  and  $\text{KNO}_3$  was chosen for further study as the most efficient and thermally stable additive. It allowed the decarbonation process to be efficiently carried out at  $T > 330\text{ }^\circ\text{C}$  and the specific useful heat of 1.6 MJ/kg-MgO in composite to be reached at  $360\text{ }^\circ\text{C}$  for 300 min of carbonation.

This paper addresses a detailed investigation of the  $(\text{Li}_{0.42}\text{K}_{0.58}\text{NO}_3)/\text{MgO}$  composites (referred to as  $(\text{LiK})\text{NO}_3/\text{MgO}$ ). The composites that have different salt content are prepared and their feasibility was evaluated under various conditions:  $T_{\text{carb.}} = 290\text{--}360\text{ }^\circ\text{C}$  and  $P(\text{CO}_2) = 50\text{--}101\text{ kPa}$ . Additionally, the specific useful heat was estimated to find an optimal salt content and cyclic experiments were also conducted to confirm the durability of material.

## 2. Experimental

### 2.1. Materials Preparation

The composite materials of lithium nitrate ( $\text{LiNO}_3$ ,  $\geq 99.0\%$  Reakhim), potassium nitrate ( $\text{KNO}_3$ ,  $\geq 99.5\%$ , Reakhim), magnesium hydroxide ( $\text{Mg}(\text{OH})_2$ ,  $\geq 99.0\%$  Reakhim) with different mixing molar ratio between  $\text{Li}_{0.42}\text{K}_{0.58}\text{NO}_3$  salt and  $\text{Mg}(\text{OH})_2$  were prepared as follows. Certain amounts of dried ( $160\text{ }^\circ\text{C}$ )  $\text{KNO}_3$  and  $\text{LiNO}_3$  were mixed with 1.0 g of  $\text{Mg}(\text{OH})_2$ . After this, some water was added to dissolve the salts and to form slurry. This slurry was dried at  $65\text{--}70\text{ }^\circ\text{C}$  by using a rotary evaporator under reduced pressure and vigorous stirring to ensure uniform distribution of the salt throughout the material. The  $(\text{LiK})\text{NO}_3/\text{MgO}$  material was prepared by dehydration of  $(\text{LiK})\text{NO}_3/\text{Mg}(\text{OH})_2$  in situ. The molar salt content in the composites,  $\alpha$  [-], was defined by the following equation, Equation (2).

$$\alpha = \frac{n(\text{Li}_{0.42}\text{K}_{0.58}\text{NO}_3)}{n(\text{Li}_{0.42}\text{K}_{0.58}\text{NO}_3) + n(\text{Mg}(\text{OH})_2)} = \frac{n(\text{Li}_{0.42}\text{K}_{0.58}\text{NO}_3)}{n(\text{Li}_{0.42}\text{K}_{0.58}\text{NO}_3) + n(\text{MgO})} \quad (2)$$

where  $n$  [mol] is the amount of a component. The  $(\text{LiK})\text{NO}_3/\text{MgO}$  composites were prepared with the salt content of 2, 5, 10, 20, and 30 mol% ( $\alpha = 0.02, 0.05, 0.10, 0.20$ , and  $0.30$ ).

### 2.2. Materials Characterization

The dynamic study of carbonation of the  $(\text{LiK})\text{NO}_3/\text{MgO}$  composites was carried out by using a TG analysis system TGD-9600 (Advance RIKO, Inc.) equipped with a flow gas control system which allowed measurements in  $\text{CO}_2$  or Ar atmosphere (Figure 2); total gas flow rate is 100 CCM for 101 kPa of total pressure. For the kinetic study of carbonation,  $(\text{LiK})\text{NO}_3/\text{Mg}(\text{OH})_2$  composites powder was loaded into the platinum cell ( $D:8\text{ mm}$ ,  $H:10\text{ mm}$ ) in order to secure same amount of MgO in composites ( $\sim 30.6\text{ mg}$  of MgO), then heated to  $350\text{ }^\circ\text{C}$  (5 K/min) and completely dehydrated at this temperature for 30 min. Then, the measuring cell was heated or cooled to the desired temperature  $T_{\text{carb.}}$  in Ar flow and switched to the flow of  $\text{CO}_2$  which initiated carbonation. Carbon dioxide was supplied to the reaction chamber for 300 min. To evaluate the carbonation reactivity of  $(\text{LiK})\text{NO}_3/\text{MgO}$  composite, reacted mole fraction,  $x$  [-], was calculated from the balance-measured sample mass change:

$$x = \frac{\Delta m}{n_0 + M_{\text{CO}_2}} \quad (3)$$

where  $\Delta m$  is the sample mass change [kg],  $n_0$  is the initial amount of MgO in the sample [mol], and  $M_{\text{CO}_2}$  is the molecular weight of  $\text{CO}_2$  [kg/mol].

The heat output performance,  $Q_{\text{comp.}}$  [kJ/kg-composite] and  $W_{\text{comp.}}$  [kW/kg-composite], of  $(\text{LiK})\text{NO}_3/\text{MgO}$  composites were also as:

$$Q_{\text{comp.}} = \frac{\Delta_r^0 H \cdot x}{M_{\text{comp.}}} \cdot (1 - \alpha) \quad (4)$$

$$W_{\text{comp.}} = \frac{dQ_{\text{comp.}}}{dt} \quad (5)$$

where the reaction enthalpy  $\Delta_r^0 H = 116.4$  kJ/mol,  $M_{\text{comp.}}$  [kg/mol] is the molar weight of (LiK)NO<sub>3</sub>/MgO composite, and  $t$  [s] is the process time.

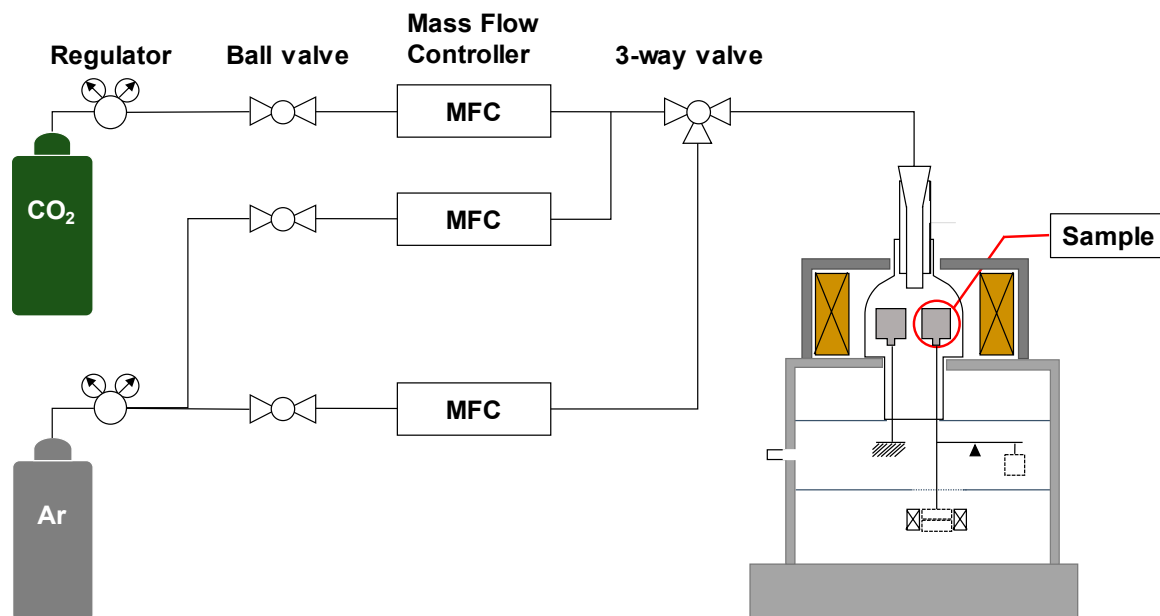


Figure 2. Schematic diagram of a TGA system (TGD-9600, Advance RIKO, Inc., Kanagawa, Japan).

### 3. Results and Discussion

The interaction of pure MgO with CO<sub>2</sub> is kinetically hindered; therefore, namely the MgO carbonation has to be accelerated to make a return of the stored heat feasible. In this work, we have optimized the salt content keeping in mind, first of all, dynamic features of the MgO carbonation reaction.

#### 3.1. Carbonation Kinetics for Various Salt Contents

For a general comparison of the new (LiK)NO<sub>3</sub>/MgO composites, for which salt content changes between 2 and 30 mol%, the isothermal carbonation was studied at 300 °C and 350 °C and  $P(\text{CO}_2) = 101$  kPa. The pure MgO undergoes no carbonation at  $T_{\text{carb.}} \leq 350$  °C (Figure 3b) and only little effect was observed at  $\alpha = 0.02$ ; however, significant acceleration of carbonation was revealed at  $\alpha \geq 0.05$ . The carbonation conversion,  $\Delta x$ , reaches 0.15–0.66 and 0.33–0.70 at 300 °C and 350 °C, respectively. It demonstrates a high sensitivity of the composite reactivity to the content of doping salt at low contents. At  $t_{\text{carb.}} < 180$  min, faster and reliable carbonation performance is observed for  $\alpha = 0.20$  compared with other materials. In contrast, for  $\alpha = 0.10$ , good performance is observed at 350 °C which significantly reduced at lower reaction temperature. For  $\alpha = 0.30$ , the carbonation performance is always lower.

Carbonation performance for composites with  $\alpha = 0.10$  and 0.20 at various CO<sub>2</sub> partial pressure and temperature was also investigated ( $T_{\text{carb.}} = 300$  °C and 350 °C,  $P_{\text{CO}_2} = 50$  kPa, 70 kPa, and 101 kPa). At  $T_{\text{carb.}} = 300$  °C, the composite with  $\alpha = 0.20$  exhibits superior carbonation performance than that with  $\alpha = 0.10$  (Figure 4a). The carbonation reactivity at  $\alpha = 0.20$  and partial CO<sub>2</sub> pressure of 50 kPa is even higher than that of  $\alpha = 0.10$  at 101 kPa (Figure 4b). At 350 °C, the composites with  $\alpha = 0.10$  and 0.20 exhibit similar carbonation reactivity at any CO<sub>2</sub> partial pressure (Figure 4b).

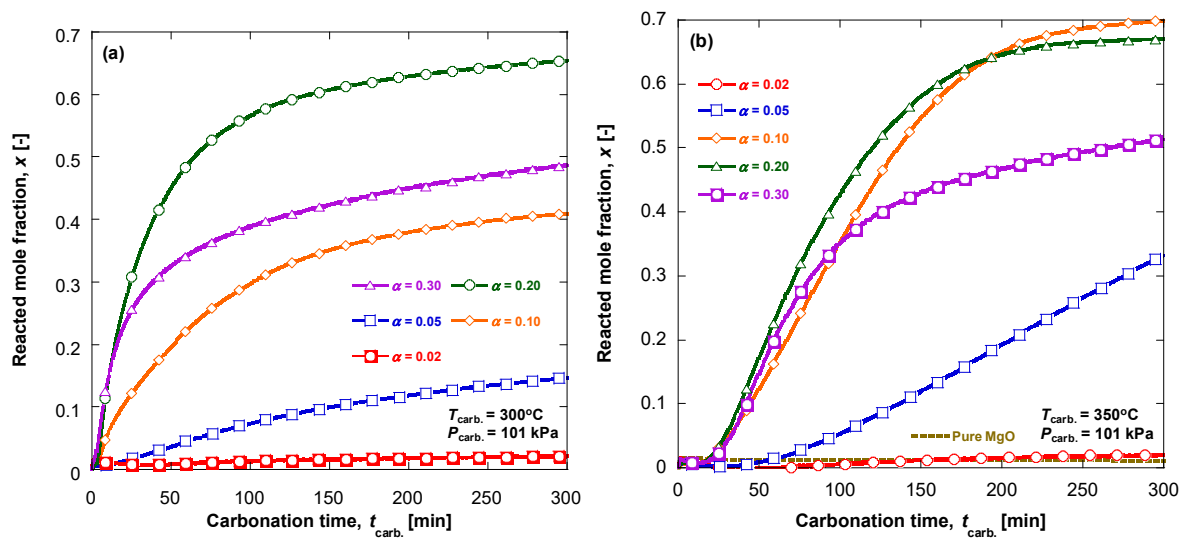


**Figure 3.** Carbonation dynamics of the (LiK)NO<sub>3</sub>/MgO composites: isothermal experimental results at (a) 300 °C and (b) 350 °C under  $P(\text{CO}_2) = 101\text{ kPa}$ .

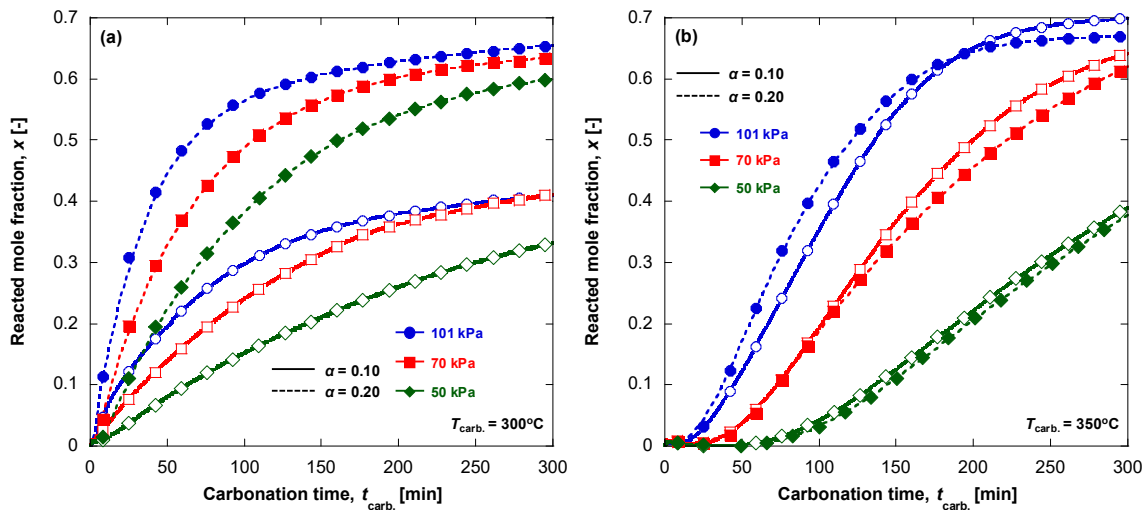


**Figure 4.** Carbonation dynamics of  $\alpha = 0.10$  (empty symbols) and  $0.20$  (bold symbols) composite under various CO<sub>2</sub> partial pressure: (a) 300 °C and (b) 350 °C.

The acceleration of carbonation is observed because the eutectic salt melts at 125 °C [22] and acts as a reaction medium in which both CO<sub>2</sub> and MgO are dissolved [21]. The dissolution of solid MgO in the molten salt and its dissociation  $\text{MgO} \rightarrow \text{Mg}^{2+} + \text{O}^{2-}$  (Figure 5) helps to overcome the high energy of the MgO lattice re- construction that results in the effective activation of the MgO toward reaction with CO<sub>2</sub> [23]. At  $\alpha = 0.02$ , volume of the liquid phase is small and the promotion effect is negligible; the carbonation of MgO was activated when  $\alpha$  is greater than 0.05 and the reactivity was maximized at  $\alpha = 0.10$ – $0.20$ . The reactivity decreases at larger  $\alpha$ , probably, because the liquid salt film on the MgO surface becomes thicker that makes the path for diffusion of CO<sub>2</sub>, Mg<sup>2+</sup> and O<sup>2-</sup> longer. Also, more melting salt surrounding MgO promotes ionization before crystallization of MgCO<sub>3</sub>.

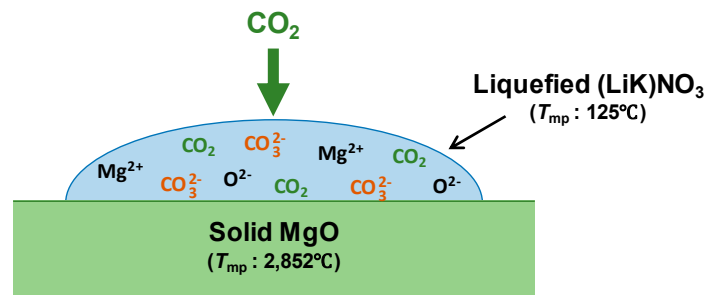


Figure 5. Carbonation mechanism of (LiK)NO<sub>3</sub>/MgO [23].

At 350 °C, all the kinetic curves are S-shaped with the induction period which significantly reduces if the salt content increases to 10 mol% and then remains almost constant (Figure 3b). According to the mentioned mechanism of the salt melting, the induction period may be attributed to the low solubility of CO<sub>2</sub> in the liquid salt film. Alternatively, this period may indicate a slow formation of critical nuclei of MgCO<sub>3</sub> phase formed in the molten salt because of insufficient super-saturation. Indeed, the duration of this period strongly depends on the system deviation from the equilibrium (see the next Section).

### 3.2. Carbonation Kinetics under Various Reaction Temperatures

To elucidate the effect of temperature on the carbonation dynamics, composites with  $\alpha = 0.05$ – $0.20$  were examined under isothermal conditions at  $T_{\text{carb.}} = 290$ – $360$  °C,  $P(\text{CO}_2) = 101$  kPa and  $t_{\text{carb.}} = 300$  min (Figure 6).

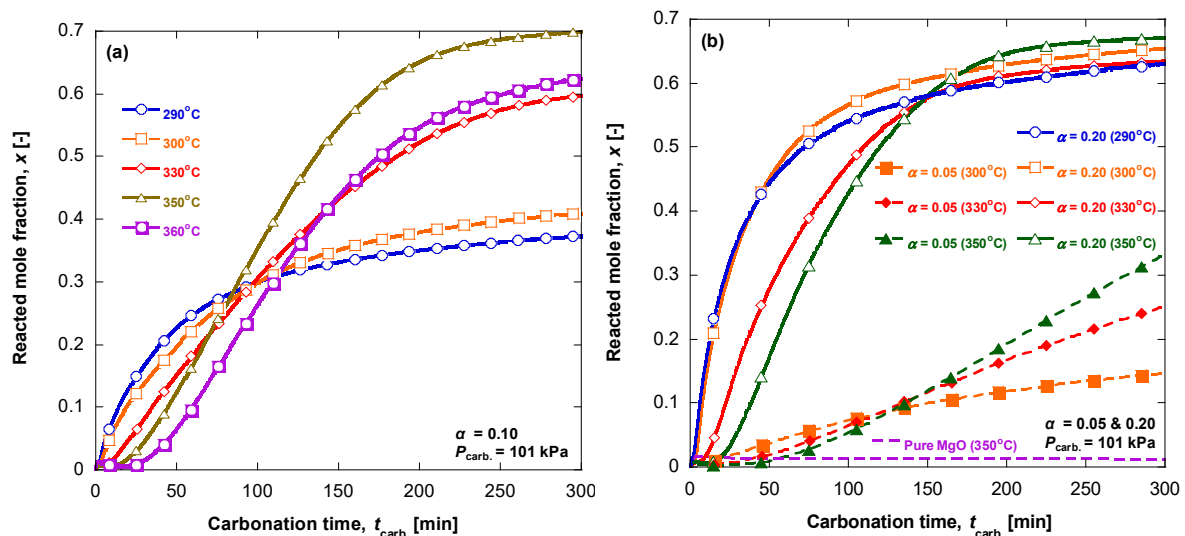


Figure 6. Carbonation kinetics of (LiK)NO<sub>3</sub>/MgO at (a)  $\alpha = 0.10$  and (b)  $\alpha = 0.05$  and  $0.20$  at various carbonation temperatures.

For all tested materials, the kinetics at low temperature (290–300 °C) are convex curves, so that the synthesis rate is maximal at  $t = 0$  and gradually decreases in time. It is quite different from the carbonation at 350 °C (Figures 3b and 4b), which initial rate is zero and the process starts after a certain induction period. This fact may denote changing carbonation mechanism or its rate-limiting step with temperature. Kinetic curves at 330 °C are intermediate between the two boundary cases. The appearance and prolongation of the induction period are accompanied with the significant increase in the final conversion  $\Delta x$  (300 min): from 0.15 to 0.33 for  $\alpha = 0.05$ , and from 0.37 to 0.70 at  $\alpha = 0.10$ . For the latter material, further enlargement of the induction period is observed at 360 °C along with the  $\Delta x$ -reduction to 0.62 (Figure 6a). Thus, the closer the carbonation temperature to the equilibrium

temperature at  $P(\text{CO}_2) = 101 \text{ kPa}$  ( $388 \text{ }^\circ\text{C}$ ) [14], the longer the induction period. Besides this factor, the complex temperature dependence of the carbonation dynamics can be due to the interplay between other influencing factors, such as

- the temperature effect on the  $\text{CO}_2$  and  $\text{MgO}$  solubilities in the melt. It is known that the  $\text{CO}_2$  solubility in a  $\text{KNO}_3$  melt passes a maximum at  $375 \text{ }^\circ\text{C}$  and reduces at the higher temperature, whereas the  $\text{CO}_2$  solubility in a  $\text{LiNO}_3$  melt gradually increases with temperature [24];
- the dependence of the  $\text{CO}_2$ ,  $\text{Mg}^{2+}$  and  $\text{O}^{2-}$  diffusivities on temperature, as their diffusion can be responsible for very slow approaching the equilibrium.

For the material with  $\alpha = 0.20$ , the final conversion is almost constant at  $290 \text{ }^\circ\text{C} \leq T_{\text{carb.}} \leq 350 \text{ }^\circ\text{C}$ , whereas the synthesis rate remarkably enhances at low temperature (Figure 6b). This material provides the high conversion (0.63–0.67) together with the good carbonation dynamics and can be recommended for TCES in this temperature range. It is worthy to mention that the carbonation conversion of 0.65–0.70, reported in this paper, is close to the maximal one's ever reported for  $\text{MgO}$ -base materials doped with salts: e.g., the  $\text{CO}_2$  uptake  $15.7 \text{ mmol/g}$  at  $340 \text{ }^\circ\text{C}$  and  $16.8 \text{ mmol/g}$  at  $300 \text{ }^\circ\text{C}$  was reported for  $\text{MgO}$  doped with  $\text{LiNO}_3$ - $(\text{NaK})\text{NO}_3$  [25] and  $(\text{LiNaK})\text{NO}_3$  [26], respectively.

### 3.3. Characterization of the Materials by SEM

The morphology of the composites was observed through scanning electron microscopy (SM-200, TOPCON Inc.) with an acceleration voltage of 7 kV. The SEM images taken at 5000 magnification indicate the hexagonal morphology of  $\text{MgO}$  crystals ( $0.5$ – $1.5 \text{ }\mu\text{m}$  size) before carbonation. At increasing salt content, the crystal border becomes fuzzier due to a thick salt layer surrounding  $\text{MgO}$  (Figure 7a,c,e,g). This fact could support the reason why too much salt decreases the reactivity. After carbonation, the particles of the product, that is a mixture ( $\text{MgCO}_3 + \text{MgO} + \text{salt}$ ), are smaller and poorly crystallized with respect to the initial ( $\text{MgO} + \text{salt}$ ) mixture (Figure 7b,d,f,h). This can be caused by the salt melting and coating of the ( $\text{MgCO}_3 + \text{MgO}$ ) crystals surface. The morphology of composite with  $\alpha = 0.20$  certainly differs from the other materials due to larger structural features formed by the salt coating (Figure 7f). This can create a better network for  $\text{CO}_2$  diffusion and facilitate reaction of  $\text{CO}_2$  with the dissolved  $\text{MgO}$ , and, therefore, to be a reason for the good dynamic performance of this material.

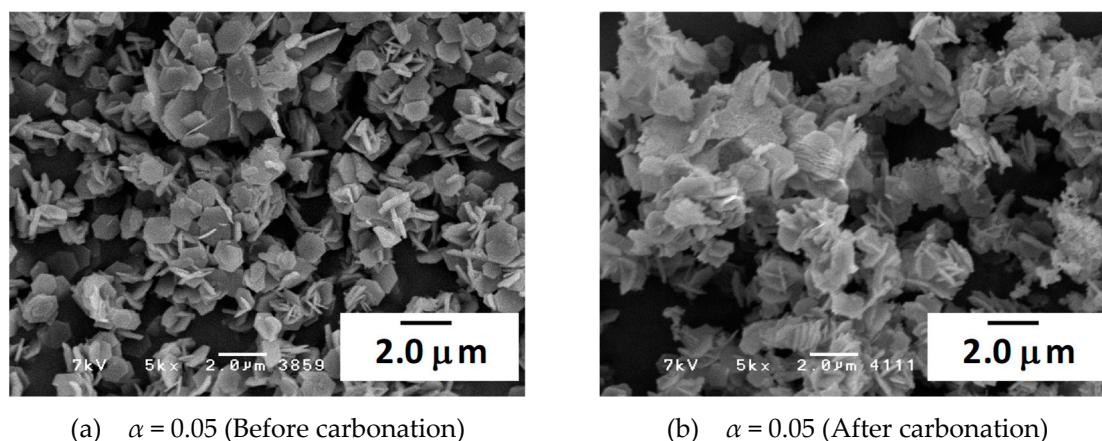
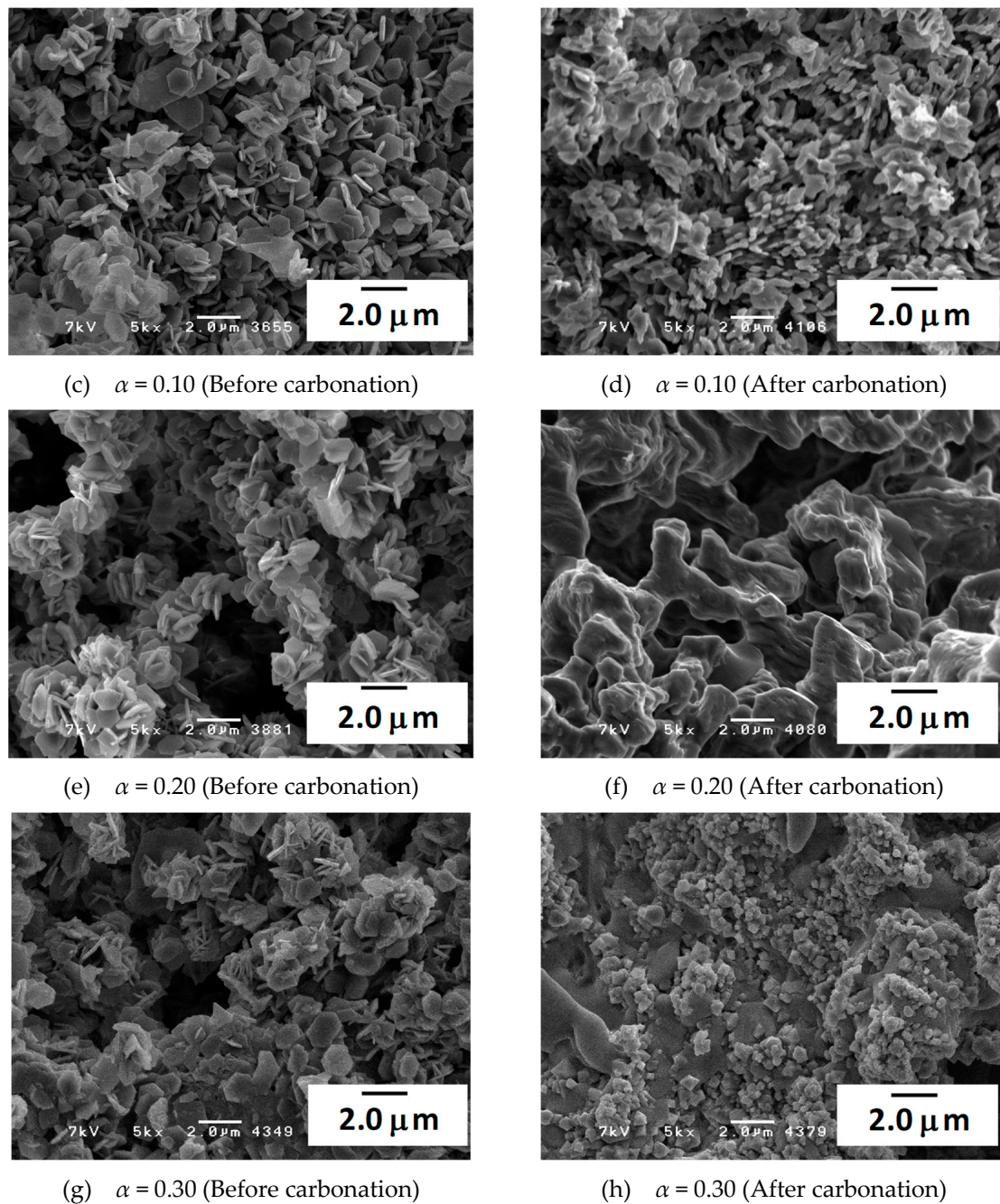


Figure 7. Cont.



**Figure 7.** SEM images of materials ( $\alpha = 0.05, 0.10, 0.20,$  and  $0.30$ ) before and after carbonation at  $350\text{ }^{\circ}\text{C}$  for 300 min.

### 3.4. Evaluation of the Specific Useful Heat

The specific useful heat and power related to unit mass of composite,  $Q_{\text{comp.}}$  and  $W_{\text{comp.}}$ , are estimated from the measured reacted mole fraction by Equations (4) and (5). At  $300\text{ }^{\circ}\text{C}$ , the  $(\text{LiK})\text{NO}_3/\text{MgO}$  composite with  $\alpha = 0.20$  exhibits larger specific useful heat  $Q_{\text{comp.}} = 1.23\text{ MJ/kg-composite}$  than the composite with  $\alpha = 0.10$  (Figure 8a), even if it contains less MgO. At  $350\text{ }^{\circ}\text{C}$ , the latter material,  $\alpha = 0.10$ , has higher  $Q_{\text{comp.}}$  value of  $1.63\text{ MJ/kg-composite}$  (Figure 8b). Both values are superior to those earlier measured for other salt/MgO composite for TCES system, namely,  $1.04\text{ MJ/kg-composite}$  and  $1.17\text{ MJ/kg-composite}$  for the  $\text{CaCl}_2$  and LiBr modified  $\text{MgO-H}_2\text{O}$  TCES material respectively [27,28].

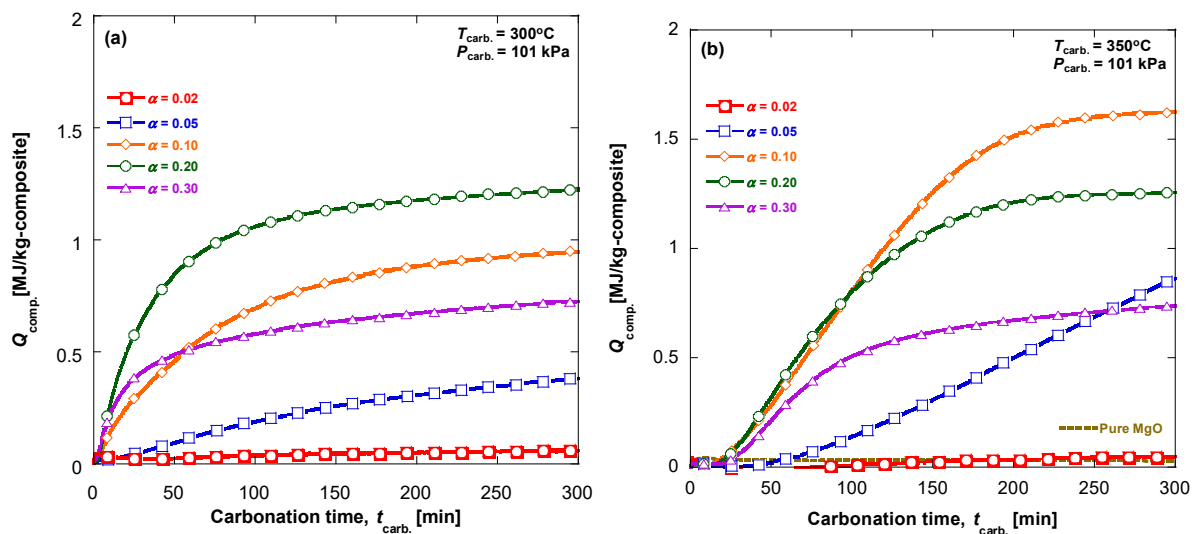


**Figure 8.** Specific useful heat,  $Q_{comp.}$ , as a function of the carbonation time at (a) 300 °C and (b) 350 °C calculated from Figure 3.

The change of maximum specific useful heat,  $Q_{comp.-max}$ , according to mixing mole ratio is displayed in Figure 9. All mixing mole ratio of (LiK)NO<sub>3</sub>/MgO composite exhibits similar reaction tendency under every temperature; the overall  $Q_{comp.-max}$  value has increased with the increasing reaction temperature, Figure 9a. It is also confirmed that  $\alpha$  of 0.05 and 0.10 (LiK)NO<sub>3</sub>/MgO composites are sensitive to reaction temperature change, on the other hand,  $\alpha$  of 0.20 and 0.30 composites, show stable results, Figure 9b.

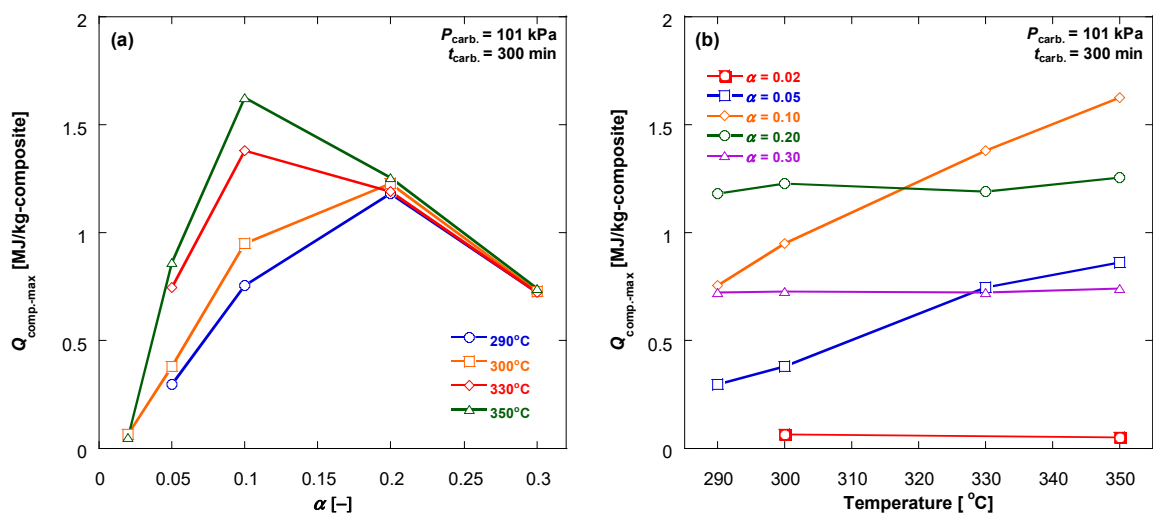


**Figure 9.** Changes of maximum specific useful heat,  $Q_{comp.-max}$ : (a)  $Q_{comp.-max}$  by salt content in the composite,  $\alpha$ , and (b)  $Q_{comp.-max}$  by carbonation temperature,  $T_{carb.}$ .

### 3.5. Evaluation of the Specific Power of Heat Release

Figure 10 shows the heat output rate,  $W_{comp.}$ , of  $\alpha = 0.10$  and  $0.20$  composites under various reaction temperature. At initial time of carbonation, both composites show high  $W_{comp.}$  values that are increased as reaction temperature decreased, but this order is changed after 50 min; carbonation under high temperature exhibits better  $W_{comp.}$  values. The highest  $W_{comp.}$  value of  $\alpha = 0.20$ ,  $0.68$  kW/kg-composite, is higher by a factor of  $\sim 2$  than that of  $\alpha = 0.10$  composite,  $0.40$  kW/kg-composite, at  $290$  °C. The composite with  $\alpha = 0.20$  shows generally higher  $W_{comp.}$  performance than  $\alpha = 0.10$  composite at low temperatures

( $\leq 330$  °C). Since its high specific useful heat capacity,  $Q_{\text{comp.}}$ , and output rate,  $W_{\text{comp.}}$ , under various reaction conditions,  $\alpha = 0.20$  is suggested as optimized mixing mole ratio for (LiK)NO<sub>3</sub>/MgO composite.

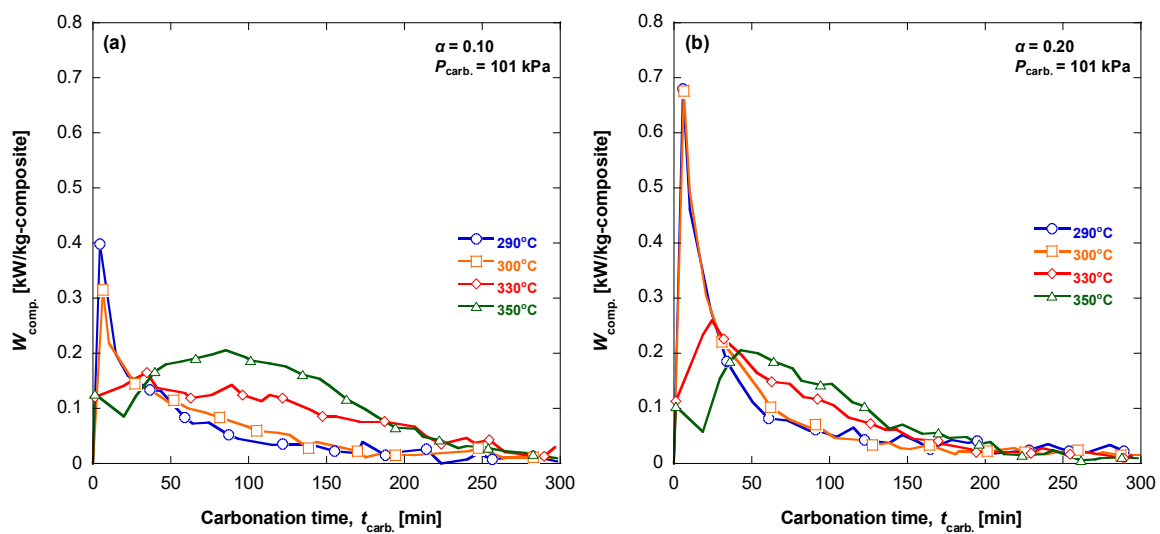


**Figure 10.** Comparison of heat output rate,  $W_{\text{comp.}}$ , under various reaction temperature: (a)  $\alpha = 0.10$ , (b)  $\alpha = 0.20$ .

#### 4. Material Durability on Cyclic Experiment

The durability of the (LiK)NO<sub>3</sub>/MgO ( $\alpha = 0.20$ ) is investigated through a cyclic experiment (Figure 11). The reacted conversion value,  $\Delta x$ , is increased for 2 cycles and becomes stabilized with increasing number of cycles;  $\Delta x$  is converged to 0.34 and that value is equivalent to 0.64 MJ/kg-composite. It is also found that decarbonation for 150 min is not enough to completely decarbonize the (LiK)NO<sub>3</sub>/MgO ( $\alpha = 0.20$ ) composite. The difference of reacted mole fraction,  $x$ , during cyclic experiment are shown in Figure 12. Carbonation reactivity is significantly increased after 1st cycle by gas diffusivity enhancement. Then carbonation reactivity and reacted conversion values are gradually getting stabilized during initial 5 cycles (Figure 12a);  $\Delta x$  value was changed from 0.58 to 0.44. However, there is no particular change in  $\Delta x$  values after 10th cycle (Figure 12b), especially 18th cycle and 20th cycle showed same reacted conversion values ( $\Delta x = 0.34$ ).

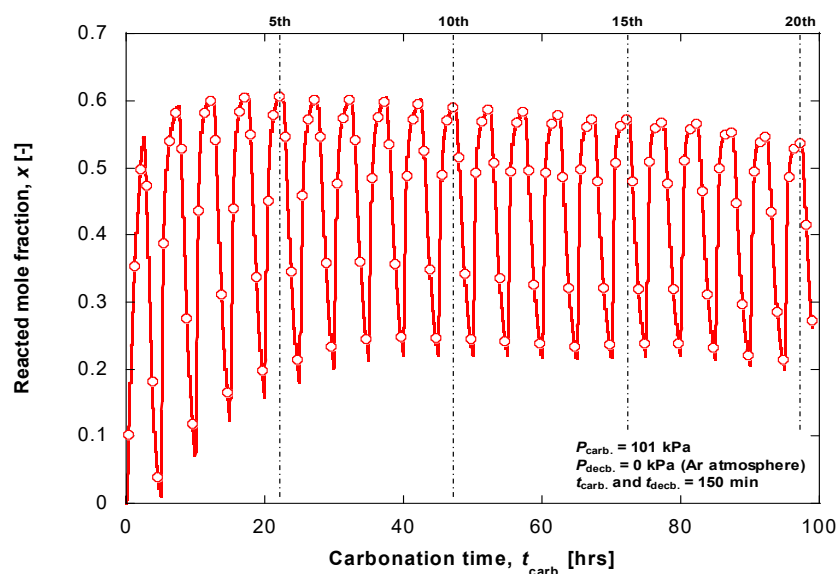


**Figure 11.** Cyclic experimental result for (LiK)NO<sub>3</sub>/MgO composite ( $\alpha = 0.20$ ) at 330 °C.

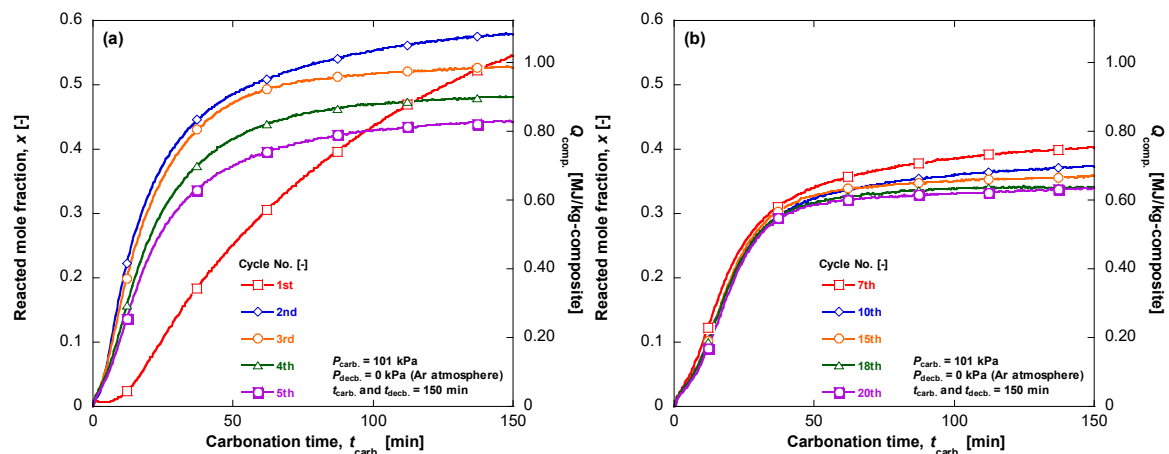


**Figure 12.** Change in the reacted mole fraction during the cyclic experiment: (a) 1st–5th cycles and (b) 7th–20th cycles.

## 5. Conclusions

The carbonation dynamics of (LiK)NO<sub>3</sub>/MgO composites, that have various molar salt content ( $\alpha = 0.02, 0.05, 0.10, 0.20, \text{ and } 0.30$ ) was investigated for effective utilizing of the medium temperature heat (300–400 °C). A set of carbonation dynamic experiments were conducted under various reaction temperature  $T = 290 \text{ °C}–360 \text{ °C}$  and CO<sub>2</sub> partial pressure  $P(\text{CO}_2) = 50–101 \text{ kPa}$  to find the optimal salt content.

The carbonation reactivity is revealed at  $\alpha > 0.05$  and reached a maximum at  $\alpha = 0.10–0.20$ . The carbonation mechanisms are suggested and SEM measurements are also conducted for understanding carbonation behavior of the (LiK)NO<sub>3</sub>/MgO composites. The specific useful heat,  $Q_{\text{comp.}}$ , was calculated from the measured reacted mole fraction,  $\Delta x$ . Despite the largest  $Q_{\text{comp.}} = 1.63 \text{ MJ/kg-composite}$  was detected at  $\alpha = 0.10$  and  $T_{\text{carb.}} = 350 \text{ °C}$ ,  $\alpha = 0.20$  was suggested as the optimal salt content because it ensures high and stable  $Q_{\text{comp.}}$  values of 1.18–1.25 MJ/kg-composite in the whole temperature range between 290 °C and 350 °C. To confirm the durability of the optimized (LiK)NO<sub>3</sub>/MgO composite ( $\alpha = 0.20$ ), cyclic experiments are conducted at 330 °C. The reacted conversion became stabilized at  $\Delta x = 0.34$  ( $Q_{\text{comp.}} = 0.64 \text{ MJ/kg-composite}$ ). The studied (Li<sub>0.42</sub>K<sub>0.58</sub>)NO<sub>3</sub> promoted MgO-CO<sub>2</sub> working pair has good potential for thermochemical storage of middle temperature heat (300–400 °C).

**Author Contributions:** Conceptualization, A.S.; Investigation, H.M.; Project administration, Y.K.; Resources, H.T. and A.S.; Supervision, Y.K. and Y.A.; Writing—original draft, S.T.K.; Writing—review & editing, Y.A. and S.T.K.

**Funding:** This research received no external funding.

**Acknowledgments:** The authors deeply appreciate the Tokyo Tech World Research Hub Initiative (WRHI) for its research support.

**Conflicts of Interest:** The authors declare no conflicts of interest.

## Nomenclature

TCES	thermochemical energy storage
TG	thermogravimetric
SEM	scanning electron microscopy
$n$	amount of a chemical compound [mol]
$n_0$	initial amount of MgO in a composite [mol]
$M_{\text{comp.}}$	molar mass of a composite [g/mol]
$Q_{\text{comp.}}$	specific useful heat [kJ/kg-composite]
$T_{\text{carb.}}$	carbonation temperature [°C]
$T_{\text{eq}}$	equilibrium transition temperature [°C]
$T_{\text{mp}}$	melting point [°C]

$W_{\text{comp.}}$	heat output [kW/kg]
$X$	reacted mole fraction, [-]
$A$	molar fraction of salt in a composite [-]
$\Delta_r^0H$	reaction enthalpy [kJ/mol]

## References

- Zsembinszki, G.; Sole, A.; Barreneche, C.; Prieto, C.; Fernández, A.I.; Cabeza, L.F. Review of reactors with potential use in thermochemical energy storage in concentrated solar power plants. *Energies* **2018**, *11*, 2358. [[CrossRef](#)]
- Gil, A.; Medrano, M.; Martorell, I.; Lázaro, A.; Dolado, P.; Zalba, B.; Cabeza, L.F. State of the art on high temperature thermal energy storage for power generation. Part 1-Concepts, materials and modellization. *Renew. Sustain. Energy Rev.* **2010**, *14*, 31–55. [[CrossRef](#)]
- Kalaiselvam, S.; Parameshwaran, R.; Kalaiselvam, S.; Parameshwaran, R. *Thermal Energy Storage Technologies for Sustainability*, 1st ed.; Elsevier Science: Amsterdam, The Netherlands, 2014; pp. 127–144. ISBN 978-0124172913.
- Lovegrove, K.; Luzzi, A.; Soldiani, I.; Kreetz, H. Developing ammonia based thermochemical energy storage for dish power plants. *Sol. Energy* **2004**, *76*, 331–337. [[CrossRef](#)]
- Shkatulov, A.I.; Aristov, Y. Thermochemical Energy Storage using  $\text{LiNO}_3$ -Doped  $\text{Mg}(\text{OH})_2$ : A Dehydration Study. *Energy Technol.* **2018**, *6*, 1844–1851. [[CrossRef](#)]
- Shkatulov, A.I.; Aristov, Y. Calcium hydroxide doped by  $\text{KNO}_3$  as a promising candidate for thermochemical storage of solar heat. *RSC Adv.* **2017**, *7*, 42929–42939. [[CrossRef](#)]
- Lutz, M.; Bhouri, M.; Linder, M.; Bürger, I. Adiabatic magnesium hydride system for hydrogen storage based on thermochemical heat storage: Numerical analysis of the dehydrogenation. *Appl. Energy* **2019**, *236*, 1034–1048. [[CrossRef](#)]
- Wentworth, W.E.; Chen, E. Simple thermal decomposition reactions for storage of solar thermal energy. *Sol. Energy* **1976**, *18*, 205–214. [[CrossRef](#)]
- Carrillo, A.J.; Gonzalez-Aguilar, J.; Romero, M.; Coronado, J.M. Solar energy on demand: A review on high temperature thermochemical heat storage systems and materials. *Chem. Rev.* **2019**, *119*, 4777–4816. [[CrossRef](#)]
- André, L.; Abanades, S.; Flamant, G. Screening of thermochemical systems based on solid-gas reversible reactions for high temperature solar thermal energy storage. *Renew. Sustain. Energy Rev.* **2016**, *64*, 703–715. [[CrossRef](#)]
- Pan, Z.H.; Zhao, C.Y. Gas–solid thermochemical heat storage reactors for high-temperature applications. *Energy* **2017**, *130*, 155–173. [[CrossRef](#)]
- Pardo, P.; Deydier, A.; Anxionnaz-Minvielle, Z.; Rougé, S.; Cabassud, M.; Cognet, P. A review on high temperature thermochemical heat energy storage. *Renew. Sustain. Energy Rev.* **2014**, *32*, 591–610. [[CrossRef](#)]
- L'vov, B.V.; Ugolkov, V.L. Kinetics of free-surface decomposition of magnesium, strontium and barium carbonates analyzed thermogravimetrically by the third-law method. *Thermochim. Acta* **2004**, *409*, 13–18. [[CrossRef](#)]
- Bhatta, L.K.G.; Subramanyam, S.; Chengala, M.D.; Olivera, S.; Venkatesh, K. Progress in hydrotalcite like compounds and metal-based oxides for  $\text{CO}_2$  capture: A review. *J. Clean. Prod.* **2015**, *103*, 171–196. [[CrossRef](#)]
- Shkatulov, A.I.; Kim, S.T.; Miura, H.; Kato, Y.; Aristov, Y.I. Adapting the  $\text{MgO-CO}_2$  working pair for thermochemical energy storage by doping with salts. *Energy Convers. Manag.* **2019**, *185*, 473–481. [[CrossRef](#)]
- Ishitobi, H.; Uruma, K.; Takeuchi, M.; Ryu, J.; Kato, Y. Dehydration and hydration behavior of metal-salt-modified materials for chemical heat pumps. *Appl. Therm. Eng.* **2013**, *50*, 1639–1644. [[CrossRef](#)]
- Shkatulov, A.I.; Krieger, T.; Zaikovskiy, V.; Chesalov, Y.; Aristov, Y.I. Doping magnesium hydroxide with sodium nitrate: A new approach to tune the dehydration reactivity of heat-storage materials. *ACS Appl. Mater. Interfaces* **2014**, *6*, 19966–19977. [[CrossRef](#)] [[PubMed](#)]
- Shkatulov, A.I.; Aristov, Y. Modification of magnesium and calcium hydroxides with salts: An efficient way to advanced materials for storage of middle-temperature heat. *Energy* **2015**, *85*, 667–676. [[CrossRef](#)]
- Yan, J.; Zhao, C.Y. First-principle study of  $\text{CaO/Ca}(\text{OH})_2$  thermochemical energy storage system by Li or Mg cation doping. *Chem. Eng. Sci.* **2014**, *117*, 293–300. [[CrossRef](#)]
- Yan, J.; Zhao, C.Y. Thermodynamic and kinetic study of dehydration process of  $\text{CaO/Ca}(\text{OH})_2$  thermochemical heat storage system with Li doping. *Chem. Eng. Sci.* **2015**, *138*, 86–92. [[CrossRef](#)]

21. Gao, W.; Zhou, T.; Gao, Y.; Louis, B.; O'Hare, D.; Wang, Q. Molten salts-modified MgO-based adsorbents for intermediate-temperature CO<sub>2</sub> capture: A review. *J. Energy Chem.* **2017**, *26*, 830–838. [[CrossRef](#)]
22. Zhang, X.; Xu, K.; Gao, Y. The phase diagram of LiNO<sub>3</sub>-KNO<sub>3</sub>. *Thermochim. Acta* **2002**, *385*, 81–84. [[CrossRef](#)]
23. Zhang, K.; Li, X.S.; Li, W.Z.; Rohatgi, A.; Duan, Y.; Singh, P.; Li, L.; King, D.L. Phase transfer catalyzed fast CO<sub>2</sub> absorption by MgO-based adsorbents with high cycling capacity. *Adv. Mater. Interfaces* **2014**, *1*, 1400030. [[CrossRef](#)]
24. Sada, E.; Katoh, S.; Yoshii, H.; Takemoto, I.; Shiomi, N. Solubility of carbon dioxide in molten alkali halides and nitrates and their binary mixtures. *J. Chem. Eng. Data* **1981**, *26*, 279–281. [[CrossRef](#)]
25. Harada, T.; Hatton, T.A. Colloidal Nanoclusters of MgO Coated with Alkali Metal Nitrates/Nitrites for Rapid, High Capacity CO<sub>2</sub> Capture at Moderate Temperature. *Chem. Mater.* **2015**, *27*, 8153–8161. [[CrossRef](#)]
26. Qiao, Y.; Wang, J.; Zhang, Y.; Gao, W.; Harada, T.; Huang, L.; Hatton, T.A.; Wang, Q. Alkali Nitrates Molten Salt Modified Commercial MgO for Intermediate-Temperature CO<sub>2</sub> Capture: Optimization of the Li/Na/K Ratio. *Ind. Eng. Chem. Res.* **2017**, *56*, 1509–1517. [[CrossRef](#)]
27. Kim, S.T.; Ryu, J.; Kato, Y. The optimization of mixing ratio of expanded graphite mixed chemical heat storage material for magnesium oxide/water chemical heat pump. *Appl. Therm. Eng.* **2014**, *66*, 274–281. [[CrossRef](#)]
28. Myagmarjav, O.; Ryu, J.; Kato, Y. Waste heat recovery from iron production by using magnesium oxide/water chemical heat pump as thermal energy storage. *ISIJ Int.* **2015**, *55*, 464–472. [[CrossRef](#)]



© 2019 by the authors. Licensee MDPI, Basel, Switzerland. This article is an open access article distributed under the terms and conditions of the Creative Commons Attribution (CC BY) license (<http://creativecommons.org/licenses/by/4.0/>).